Journal of Natural Gas Chemistry 13(2004)23–35

SCIENCE PRESS

Screening of MgO- and CeO_2-Based Catalysts for Carbon Dioxide Oxidative Coupling of Methane to C_{2+} Hydrocarbons

Istadi*, Nor Aishah Saidina Amin**

Chemical Reaction Engineering Group (CREG), Faculty of Chemical and Natural Resources Engineering, Universiti Teknologi Malaysia, UTM Skudai, Johor Bahru, 81310 Malaysia

[Manuscript received February 13, 2004; revised March 16, 2004]

Abstract: The catalyst screening tests for carbon dioxide oxidative coupling of methane (CO_2-OCM) have been investigated over ternary and binary metal oxide catalysts. The catalysts are prepared by doping MgO- and CeO_2-based solids with oxides from alkali (Li_2O), alkaline earth (CaO), and transition metal groups (WO_3 or MnO). The presence of the peroxide (O_2^{2-}) active sites on the Li_2O_2, revealed by Raman spectroscopy, may be the key factor in the enhanced performance of some of the Li_2O/MgO catalysts. The high reducibility of the CeO_2 catalyst, an important factor in the CO_2-OCM catalyst activity, may be enhanced by the presence of manganese oxide species. The manganese oxide species increases oxygen mobility and oxygen vacancies in the CeO_2 catalyst. Raman and Fourier Transform Infra Red (FT-IR) spectroscopies revealed the presence of lattice vibrations of metal-oxygen bondings and active sites in which the peaks corresponding to the bulk crystalline structures of Li_2O, CaO, WO_3 and MnO are detected. The performance of 5%MnO/15%CaO/CeO_2 catalyst is the most potential among the CeO_2-based catalysts, although lower than the 2%Li_2O/MgO catalyst. The 2%Li_2O/MgO catalyst showed the most promising C_{2+} hydrocarbons selectivity and yield at 98.0% and 5.7%, respectively.

Key words: catalyst screening, carbon dioxide, oxidative coupling, methane, ternary metal oxide, binary metal oxide, MgO, CeO_2, C_{2+} hydrocarbons

1. Introduction

The direct conversion of methane to ethane, ethylene and acetylene (C_{2+} hydrocarbons) is considered to be one of the most effective uses of natural gas as a chemical resource. The compositions of natural gas from the Natuna's fields contains up to 71% carbon dioxide and 28% methane [1]. The high CO_2/CH_4 ratio in Natuna's natural gas compositions should be strategically utilized for the production of higher hydrocarbons and other important chemicals. It is highly desirable from the environmental point of view to utilize and convert both methane and carbon dioxide from natural gas into higher value-added chemicals without having to separate the carbon dioxide first.

Carbon dioxide rather than oxygen may be the alternative oxidant for the catalytic reaction of methane to produce C_{2+} hydrocarbons due to the fact that in the gas phase the methyl radicals are induced by the presence of oxygen and not by carbon dioxide [2,3]. Recently, the conversion of natural gas using carbon dioxide as the oxidant has received considerable attention [2–8]. Among 30 metal oxides studied, praseodymium and terbium oxides showed potential [2,3,5] for catalyzing the CO_2-OCM reaction to produce C_{2+} hydrocarbons. Carbon dioxide showed a positive role in the formation of C_{2+} hydro-

** Corresponding author. Tel: 607-5535588; Fax: 607-5581463; E-mail: r-naishah@utm.my;

* Present address: Dept. of Chemical Engineering, Diponegoro University, J1. Prof. H. Sudharto, SH., Tembalang, Semarang, 50239 Indonesia.

carbons in the oxidative coupling of methane over a PbO-MgO catalyst [5]. A series of binary metal oxide catalysts based on CaO-CeO_2 [5], CaO-ZnO [7] and La_2O_3-ZnO [9] were developed, but the catalytic performance was not satisfactory. The modification of binary metal oxide system was also developed by combining MnO_2 with alkaline earth (CaO, SrO and BaO), while Cr_2O_3, CeO_2 and ZnO were also used to replace MnO_2 [4], but the catalytic performance was again not satisfactory. In a more recent development, C_{2+} hydrocarbons selectivity approached 79.1% over Mn-$SrCO_3$ catalyst with a C_{2+} hydrocarbons yield of 4.5% [8] that closely resembled the results achieved by previous researchers [4,5,7].

Table 1 compares the screening results reported by previous researchers [4,6,8]. Most of the catalysts reported gave a lower methane conversion and a smaller C_{2+} hydrocarbons yield relatively when carbon dioxide, instead of oxygen, is the oxidant for oxidative coupling of methane. Previously, most researchers concluded that the oxidation/reduction reactions of Ce^{4+}/Ce^{3+} or Mn^{3+}/Mn^{2+} are effective to activate carbon dioxide to form oxygen active species, while the C_{2+} selectivity is related to the basicity of a catalyst due to enhanced CO_2 chemisorptions on the catalyst surface [4,5,8].

Table 1. Catalysts performance results from previous researchers

Catalysts	CH_4 conversion (%)	CO selectivity (%)	C_{2+} hydrocarbons Selectivity (%)	C_{2+} hydrocarbons Yield (%)	Ref.
CeO_2	12	—	0.5	0.1	[6]
CaO-CeO_2(Ca/Ce=0.1)	5.1	—	46	2.3	[6]
CaO-CeO_2(Ca/Ce=0.2)	4.9	—	55	2.7	[6]
CaO-CeO_2(Ca/Ce=0.5)	5	—	62	3.2	[6]
CaO-CeO_2(Ca/Ce=1)	3.4	—	46	1.6	[6]
CaO	0.3	—	36	0.1	[6]
CaO-ZnO(Ca/Zn=0.5)	3.4	18	82	2.8	[7]
CaO-MnO(Ca/Mn=1)	3.9	32	68	2.7	[4]
SrO-MnO(Sr/Mn=1)	3.9	15	85	3.3	[4]
BaO-MnO(Ba/Mn=0.5)	3.8	33	67	2.6	[4]
BaO-MnO(Ba/Mn=1)	2.3	15	85	1.9	[4]
MnO-$SrCO_3$(Mn/Sr=0.2)	5.7	79.1	20.9	4.5	[8]
MnO-$SrCO_3$(Mn/Sr=0.1)	4.9	87.9	12.1	4.3	[8]

Thermodynamic calculations for the overall reaction of CO_2-OCM demonstrated the equilibrium yields of ethane and ethylene formed by the reactions between methane and carbon dioxide were 15% and 25%, respectively, at temperature equal to and above 800 ℃ for CO_2/CH_4 ratio of 2 [4]. In another study, the equilibrium conversions of methane to ethane and ethylene were about 6% each at the same CO_2/CH_4 ratio but temperature of 600 ℃ [5]. Equations (1) and (2) are the two main reaction schemes for CO_2-OCM to produce C_{2+} hydrocarbons with carbon monoxide and water as the by-products.

$$2CH_4 + CO_2 \Longleftrightarrow C_2H_6 + CO + H_2O$$

$$\Delta H^0_{298} = +17 \text{ kJ/mol} \tag{1}$$

$$2CH_4 + 2CO_2 \Longleftrightarrow C_2H_4 + 2CO + 2H_2O$$

$$\Delta H^0_{298} = +176 \text{ kJ/mol} \tag{2}$$

Although lithium-doped magnesium oxide catalyst, Li_2O/MgO, is one of the most extensively studied catalysts for methane oxidative coupling by oxygen (O_2-OCM) [10,11], its potential in the catalytic CO_2-OCM process has not been widely studied. According to previous researchers, one of the active sites for initial abstraction of hydrogen atom from methane were believed to be $[Li^+O^-]$ ($=[Li'_{Mg}O^{\bullet}_{O}]$) centers formed by the substitution of Li^+ at lattice sites normally occupied by Mg^{2+} which was observed by EPR and XPS [11–13]. The Li^+-ion was incorporated into the MgO lattice as substitutional ions on magnesium sites with oxygen vacancies for charge compensation. The oxygen vacancies are then substituted by oxygen or carbon dioxide producing oxygen active species. Besides, it was also suggested [12,13] that a diatomic species of peroxide (O_2^{2-}) ion is also an active species on this catalyst. Since the O-O stretching mode is Raman active, Raman spectroscopy is particularly suitable for investigating peroxide species on the catalysts. However, the peroxide (O_2^{2-}) ions cannot be detected by EPR because they are diamagnetic.

CeO_2 is a basic oxide having excellent redox properties owing to the very fast reduction of Ce^{4+} to Ce^{3+} associated with the formation of oxygen vacancies at the surface and in the solid. The oxygen mobility, reducibility and ionic conductivity of CeO_2-based catalyst can be enhanced by doping CeO_2 with transition metal oxide (MnO or WO_3). The catalyst surface with a high basicity lead to the adsorption and activation of carbon dioxide to produce oxygen active species which in turn activate methane to produce methyl radicals (CH_3^*). A highly basic catalyst is proposed to be able to enhance carbon dioxide adsorption which is then activated on oxygen vacancies to form oxygen active species and gaseous carbon monoxide according to Equations (3) and (4) using the Kröger-Vink notation [13].

$$V_o^{\bullet\bullet} + 2CO_{2(gas)} \Longleftrightarrow 2O_o^{\bullet} + 2CO_{(gas)} \qquad (3)$$

$$V_o^{\bullet\bullet} + 2CO_{2(gas)} \Longleftrightarrow 2O_o^{x} + 2CO_{(gas)} + 2h^{\bullet} \qquad (4)$$

In reactions (3) and (4), $V_o^{\bullet\bullet}$ denotes doubly ionized oxygen vacancies, $h^{\bullet}$ denotes electron holes, O_o^x denotes oxygen ion on neutral lattice positions and $O_o^{\bullet}$ denotes single ionized oxygen on oxygen vacancies as active oxygen species. The reducibility and existence of defect sites on CeO_2 structures enhanced by doping CeO_2 with transition metals such as Zn, W or Mn increased oxygen vacancy centers which may be responsible for CO_2 activation to oxygen active species and, moreover, improved the catalyst surface area due to reduced CeO_2 crystal sizes [7].

In this paper, highly basic MgO- and CeO_2-based catalysts are screened to investigate their potentials in catalyzing CO_2-OCM process to produce C_{2+} hydrocarbons. Solutions of W, Mn, Ca and/or Li are impregnated on either MgO or CeO_2 to form binary and ternary metal oxide catalysts and tested for CO_2-OCM reactions. The adsorbed carbon dioxide is proposed to be activated on the oxygen vacancies to form gaseous CO and oxygen active species by reduced cerium, manganese and/or tungsten ions and also the active centers of the Li_2O/MgO catalyst. The catalysts performances for the CO_2-OCM are discussed based on their catalytic activities. In addition, the presence and the structures of metal oxides as well as the active sites on the catalyst surface are investigated by Raman and FT-IR spectroscopies.

2. Experimental

2.1. Catalyst preparation

All binary and ternary metal oxide catalysts used in this study were prepared by the conventional wet-impregnation method. CeO_2 (MERCK) or MgO (97%, MERCK) powder were used as catalyst supports, while $LiNO_3$ (99.995%, MERCK), $(NH_4)_6W_{12}O_{40} \cdot xH_2O$ (85%, FLUKA), $Mn(NO_3)_2{\cdot}4H_2O$ (98.5%, FLUKA) and/or $Ca(NO_3)_2{\cdot}4H_2O$ (99%, ALDRICH) were used as precursors. Powdery CeO_2 or MgO were first immersed into an aqueous solution of $M(NO_3)_n \cdot xH_2O$ (M=Ca, Li and Mn) or $(NH_4)_6W_{12}O_{40} \cdot xH_2O$ for 6 h at ambient temperature. The water was then evaporated overnight in an oven (MEMMERT) at 120 ℃. Next, the powder was calcined at 850 ℃ in a muffle furnace (CARBOLITE) for 4 h and then crushed into the desired size (45–60 mesh). The ternary metal oxides were prepared by sequential wet-impregnation technique. The CeO_2-based catalysts tested were pure CeO_2, 5%MnO/CeO_2, 15%CaO/CeO_2, 5%MnO/15%CaO/CeO_2 and 3%WO_3/15%CaO/CeO_2 catalysts. The amount of MnO, CaO and WO_3 loaded on the catalysts are based on previous studies [4–7] and pre-exploratory tests in which the promising catalytic performances were reported over the catalysts with these compositions. Meanwhile, pure MgO and MgO doped with 1%, 2%, 5% and 10% of Li_2O as well as 3% and 5% of WO_3 and MnO, respectively were also tested. These catalysts were also prepared according to the previous study [12] in which Li loading range of 0.5%–7.5% gave more promising results for O_2-OCM due to the suitable formation of [Li^+O^-] or peroxide ions active centers.

2.2. Catalytic reaction

All the catalytic performances were tested using a fixed-bed quartz reactor. The schematic diagram of the experimental set-up is shown in Figure 1. Before reaction, the catalyst was recalcined at 850 ℃ in air flow (100 ml/min) for 1 h and flushed with high purity nitrogen (>99.999%, 100 ml/min) at 850 ℃ for another 1 h. The reaction was initiated by feeding methane (>99.999%) and carbon dioxide (>99.995%) to the reactor. The following inlet conditions were used for the CO_2-OCM reaction during catalyst screening: T(reactor temperature)=850 ℃, CO_2/CH_4=2, F(total flow rate)=100 ml/min, W(catalyst amount)=2 g for CeO_2-based catalysts (F/W=3000 ml/(g·h)) and 0.5 g for MgO-based catalysts (F/W=12000 ml/(g·h)). The gas flow rates were measured and controlled by volumetric flow controllers (Alicat Scientific, Inc.). The products and unreacted gases were analyzed by an online gas chromatography (HP AGILENT 6890 series) equipped with a thermal conductivity detector (TCD), PORAPAK N packed-column and Chemstation software. Catalytic performance data for 4 h time on stream of reaction are reported which is an average value during the reaction time on stream. The data after 30 min of reaction time on stream are given in this paper. One analytical run was complete within 30 min and thus the sampling was repeated every 30 min.

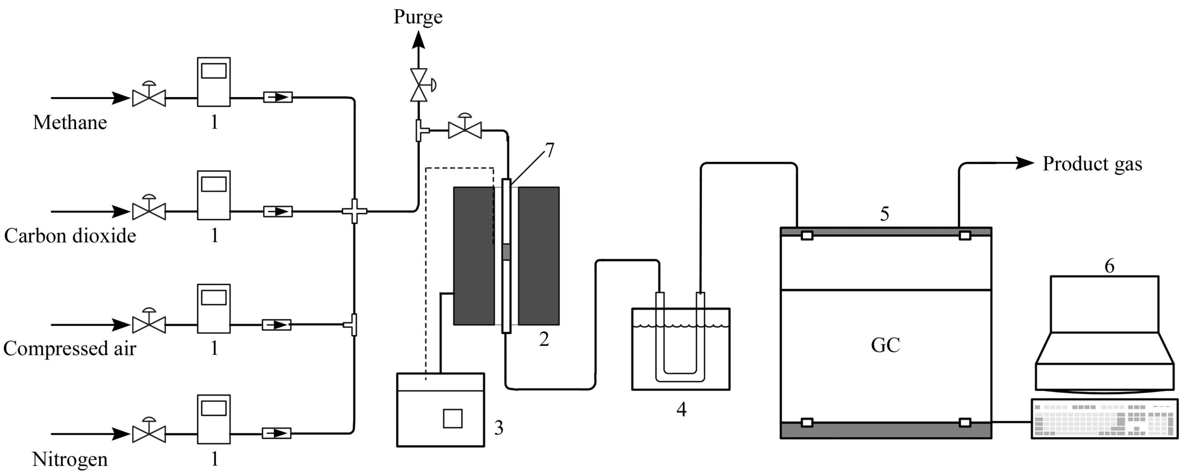

Figure 1. Schematic diagram of experimental set-up
1—Volumetric flow controller, 2—Furnace, 3—Furnace temperature controller, 4—Condenser, 5—HP Agilent GC 5890 Series, 6—Computer online for GC, 7—Fixed bed quartz reactor

Accordingly, the calculations for conversion, selectivity and yield are based on the work reported by previous researchers [2,3,6]. The gas chromatographic data were handled according to the following assumptions: (1) carbon in carbon dioxide was only converted into carbon monoxide; (2) carbon and/or hydrogen in methane were only converted into ethane, ethylene, acetylene and carbon monoxide and/or hydrogen and water, respectively; (3) therefore carbon monoxide was produced from both carbon dioxide and methane. The carbon monoxide from methane is first calculated according to the method described elsewhere [2,3,6], in which almost all of the reactions involving methane and carbon monoxide are taken into account. Therefore, conversion, selectivity and yield of C_{2+} hydrocarbons are expressed on the basis of carbon in methane as defined in Equations (5)–(7), respectively [2,3,5]. The notations of $[C_2H_4]$, $[C_2H_6]$, [CO from CH_4] and $[CH_4]$ in the following equations denote the number of moles of C_2H_4, C_2H_6, CO from CH_4, and CH_4, respectively.

$$\mathrm{CH_4\ conversion} = \frac{2[\mathrm{C_2H_4}] + 2[\mathrm{C_2H_6}] + [\mathrm{CO\ from\ CH_4}]}{[\mathrm{CH_4}] + 2[\mathrm{C_2H_4}] + 2[\mathrm{C_2H_6}] + [\mathrm{CO\ from\ CH_4}]} \times 100\% \tag{5}$$

$$\mathrm{C_{2+}\ hydrocarbons\ selectivity} = \frac{2[\mathrm{C_2H_4}] + 2[\mathrm{C_2H_6}]}{2[\mathrm{C_2H_4}] + 2[\mathrm{C_2H_6}] + [\mathrm{CO\ from\ CH_4}]} \times 100\% \tag{6}$$

$$\mathrm{C_{2+}\ hydrocarbons\ yield} = \mathrm{CH_4\ conversion} \times \mathrm{C_{2+}\ hydrocarbons\ selectivity} \times 100\% \tag{7}$$

2.3. Catalyst characterization techniques

The bulk characterization of the catalysts surface structure was carried out using Raman and FT-IR spectroscopies to investigate the presence and the structures of metal oxides or metal-oxygen bonding on the catalyst surface. The Laser Raman spectroscopy technique utilized a Perkin Elmer Spectrum GX NIR FT-Raman apparatus equipped with a Nd:YAG laser source. Initially, powdered catalyst sample was pressed into the sample holder. The Raman spectra were measured on the 2 cm^{-1} spectral resolution with an absolute accuracy of $\pm 0.1\ cm^{-1}$. Meanwhile, the excitation line was set at 514.4 nm and the excitation power was constant at 350 mW for all samples except for the Mn-based samples. For the Mn-based samples, the power attempted was in the range of 25–500 mW in order to detect the peak measurement. The Raman shift band of the sample was initially performed in the range of 4000 cm^{-1} up to 100 $cm^{-1}$and later to 1200–100 cm^{-1}, depending on the metal oxide catalyst.

The infra red spectra were recorded on a Perkin Elmer Spectrum GX NIR FT-Raman using the KBr film technique. IR spectra were acquired in the absorbance mode at 25 ℃ and resolution of 2 cm^{-1}. The IR wavenumber of the sample was initially performed in the range of 4000-400 cm^{-1} which was then focused in the range of 1000–400 cm^{-1}. The film was made by pressing about 10 mg of fine catalyst powder mixed physically with about 350 mg KBr powder. Finally, the transparent film was placed in a ring type sample holder and transferred into the IR cell.

The FT-IR and Raman spectroscopies are able to characterize the molecular structure of the surface metal oxides, the surface coverage of the metal oxide and the structure of the active surface metal oxide species during catalytic reactions. Thus, Raman spectroscopy is better suited than infra red spectroscopy to detect the molecular vibration of surface metal oxide species on certain oxide supports in the lower wavenumber region (location of M-O and M-O-M bonds). Fortunately, both Raman and infra red spectroscopy can generally provide complementary molecular vibrational information about the surface metal oxide species on the oxide supports in the higher wavenumber region (location of M=O bonds) [14,15].

3. Results and discussion

3.1. MgO-based catalysts screening for CO_2-OCM

The performances of selected binary and ternary metal oxide catalysts for CO_2-OCM over MgO-based catalysts are presented in Table 2. Among all the MgO-based catalysts tested, the highest C_{2+} hydrocarbons yield is achieved over the 2%Li_2O/MgO catalyst. For pure MgO catalyst, the methane conversion, C_{2+} hydrocarbons selectivity and yield are 5.3%, 67.3% and 3.6%, respectively. Addition of 1%Li_2O to pure MgO markedly improves the selectivity and yield of C_{2+} hydrocarbons to 90.7% and 5.3%, respectively, as revealed in Table 2. Further increase of the Li_2O content to 2%, increase the C_{2+} hydrocarbons selectivity and yield to 98.0% and 5.7%, respectively, while the methane conversion remains at 5.8%.

Table 2. Catalysts performance results of MgO-based catalyst

Catalysts	CH_4 conversion (%)	CO selectivity (%)	C_{2+} hydrocarbons	
			Selectivity (%)	Yield (%)
MgO	5.3	32.7	67.3	3.6
1%Li_2O/MgO	5.8	9.3	90.7	5.3
2%Li_2O/MgO	5.8	2.0	98.0	5.7
5%Li_2O/MgO	3.6	2.7	97.3	3.5
10%Li_2O/MgO	1.2	24.9	75.1	0.9
5%MnO/MgO	8.2	81.1	23.9	1.9
5%MnO/1%Li_2O/MgO	7.2	86.0	14.0	1.0
5%MnO/5%Li_2O/MgO	5.4	27.7	72.3	3.9
3%WO_3/1%Li_2O/MgO	1.7	21.6	78.4	1.4

A further increment of the Li_2O content from 2% to 5% resulted in a slight decrease in the C_{2+} hydrocarbons selectivity from 98.0% to 97.3%. Likewise, the methane conversion and C_{2+} hydrocarbons yield also decrease from 5.8% to 3.6% for methane conversion and from 5.7% to 3.5% for C_{2+} hydrocarbons yield. Finally, when the Li_2O content is increased to 10%, the methane conversion, C_{2+} hydrocarbons selectivity and yield decrease drastically to 1.2%, 75.1% and 0.9%, respectively.

The impact of various metal oxides doping onto the MgO-based catalysts on the catalytic performances is further presented in Table 2. The doping of 5%MnO to the pure MgO catalyst helps to increase the conversion from 5.3% to 8.2% but the yield of the C_{2+} hydrocarbons is low at 1.9% owing to a low C_{2+} selectivity at 23.9%. The effects of loading a third metal oxide to the binary metal catalyst on the catalyst activity vary. The addition of transition metals species (tungsten or manganese) to the Li_2O/MgO catalyst may distort the defect structure of the catalysts due to the large differences in the ionic radii of the manganese (0.091 nm) and the tungsten (0.065 nm) ions to that of the lithium (0.078 nm) and the magnesium (0.078 nm) ions. As a result, the amount of tungsten or manganese oxides added to the 1%Li_2O/MgO catalyst may cause a decrease in the active species concentration of $[Li^+O^-]$ centers or peroxide (O_2^{2-}) ions [11]. Tungsten addition to the Li_2O/MgO catalyst however, gives better C_{2+} hydrocarbons selectivity than that of manganese species probably due to the proximity of the tungsten ionic radius with lithium and magnesium ionic radii compared with the manganese ionic radius. From Table 2, doping 3%WO_3 to the 1%Li_2O/MgO catalyst drastically decrease the methane conversion from 5.8% to 1.7% and the C_{2+} hydrocarbons selectivity from 90.7% to 78.4%. In contrast, doping 5% of MnO to the 1%Li_2O/MgO catalyst increase the methane conversion slightly from 5.8% to 7.2%, but the C_{2+} hydrocarbons selectivity decrease from 90.7% to 14%.

Although the highest methane conversion is achieved over the 5%MnO/MgO catalyst, possibly due to the role of Mn species, the selectivity and consequently the yield of the C_{2+} hydrocarbons are very low over the binary and ternary metal oxide catalyst containing MnO. The low amount of 1%Li_2O content and the presence of MnO in the 5%MnO/1%Li_2O/MgO catalyst possibly distort the active sites for oxygen vacancies and fails to improve the C_{2+} hydrocarbons yield and selectivity considerably. At higher concentration of Li content in the ternary metal oxide catalyst, the C_{2+} selectivity and yield improve significantly indicating an optimum amount of the Li_2O content is needed to activate the ternary metal oxide catalyst. For example, increasing the Li_2O content to 5% in the 5%MnO/5%Li_2O/MgO improves the C_{2+} selectivity from 14% to 72.3% and the yield from 1% to 3.9% although the conversion decreases slightly from 7.2% to 5.4% over the ternary metal oxide catalyst. The addition of Mn species to the Li_2O/MgO however, is not able to improve the selectivity and the yield of the C_{2+} hydrocarbons. This is apparent in the decrement of the C_{2+} selectivity and yield after 5%MnO is added to the 5%Li_2O/MgO catalyst. Indeed, based on the C_{2+} hydrocarbons yield and selectivity, the 2%Li_2O/MgO and the 5%MnO/1%Li_2O/MgO catalysts exhibit the highest and lowest performances, respectively as revealed in Table 2.

The presence and structures of surface metal oxides and the peroxide (O_2^{2-}) ions centers, believed to be one of the active site species [12,16], are indicated by Raman and FT-IR spectroscopies. The Raman and FT-IR results of MgO-based catalysts including the corresponding vibration modes are briefly listed in Table 3 and are presented in Figures 2–5. Figure 2 reveals the Raman spectra of fresh and used 2%Li_2O/MgO catalyst as well as pure MgO in the band region of 1200–200 cm^{-1}, while Figure 3 compares the peaks of fresh and used tungsten oxide-doped Li_2O/MgO catalysts including their relationships with pure MgO and Li_2O/MgO catalysts. This comparison is aimed to investigate the effect of WO_3 doping on the catalyst structure. The FT-IR spectra of pure MgO, 1%Li_2O/MgO, 2%Li_2O/MgO and 5%Li_2O/MgO catalysts are compared in Figure 4, while the tungsten oxide doping effect on 1%Li_2O/MgO catalyst are presented in Figure 5.

The promising performance given by the 2%Li_2O/MgO catalyst in producing C_{2+} hydrocarbons may be due to increasing oxygen vacancies from the peroxide (O_2^{2-}) ions and $[Li^+O^-]$ centers formed by incorporation of Li^+-ions into the MgO lattice. The Li^+-ions took action as substitutional ions on Mg sites with oxygen vacancies for charge compensation with the closely ionic radius of Li^+ (0.078 nm) to Mg^{2+} (0.078 nm). In the Kröger-Vink notation this can be written in Equation (8) [13].

$$\text{"}Li_2O\text{"} + 2Mg_{Mg}^{x} + O_o^{x} \Longleftrightarrow 2Li'_{Mg} + V_o^{\bullet\bullet} + 2\text{"}MgO\text{"} \quad (8)$$

where "Li_2O" and "MgO" represent the incoming lithium oxide and the displaced magnesium oxide, respectively. It is proposed that adsorption of gaseous carbon dioxide on oxygen vacancies give active oxygen species and gaseous carbon monoxide as abovementioned in Equations (3) and (4). From the possible mechanism Li'_{Mg} means Li^+ dopant ions substituted on Mg sites, while $O_o^{\bullet}$ means oxygen dopant ion on O sites. In terms of defect, the notation of $[Li'_{Mg}O_o^{\bullet}]$ which is preferred to denote as $[Li^+O^-]$, is the associated pair of one Li^+-ion and one O^--ion that is thought to be responsible for the catalytic activity by the hydrogen atom abstraction from methane. In order to make Li_2O/MgO catalyst catalytically active the presence of oxygen atom is necessary. In terms of defect chemistry this means that in the oxidation of the oxygen vacancies, holes states are formed according to Equations (3) or (4) [13] using Kröger-Vink notation. The localized hole states may be described as or $2(O^{-}{=}O_o^{\bullet})$ or $O_2^{2-}{=}(O_2)_o^{\bullet\bullet}$ [13]. The most probable origin of the electron is the contribution of an electron from lattice oxygen, O_o^x, under the formation of an electron hole, present as an $O_o^{\bullet}$-ion.

Table 3. Resume of Raman and FT-IR spectra of 2%Li_2O/MgO and 3%WO_3/1%Li_2O/MgO catalysts

Materials	Band positions (cm^{-1})		Vibration modes	Structures	Ref.
	Raman	FT-IR			
2%Li_2O/MgO	689, 1086	—	CO_3^{2-} symmetric stretching	crystalline Li_2CO_3	[12]
	761	—	CO_3^{2-} antisymmetric bending	crystalline Li_2CO_3	[12]
	860–794, 259	—	O-O stretching of O_2^{2-}	crystalline Li_2O_2	[12]
	426, 500, 575	—	—	crystalline Li_2O	[12]
	—	460–430	Li-O antisymmetric stretching	[LiO_4] tetrahedral	[19,21]
	—	546, 507	—	crystalline Li_2O	[19,21]
3%WO_3/1%Li_2O/MgO	798, 816	—	O-O stretching of O_2^{2-}	crystalline Li_2O_2	[12]
	422, 510, 520	—	—	crystalline Li_2O	[12]
	751	—	—	crystalline Li_2CO_3	[12]
	918	—	W-O symmetric stretching	[WO_4] tetrahedral	[17]
	279	—	W-O-W deformation	crystalline WO_3	[17,20]
	553	862–817	W=O stretching	[WO_6] octahedral	[17,22]
	980	—	W-O symmetric stretching	crystalline $MgWO_4$	[17]
	353, 355	—	W-O bending	distorted [WO_4] tetrahedral	[17]
	—	688	O-W-O stretching	—	[22]
	—	432	Li-O stretching	[LiO_4] tetrahedral	[19,21]

The peroxide (O_2^{2-}) ion proposed to be one of the active species of the Li_2O/MgO catalyst for oxidative coupling of methane can be indicated by Raman spectroscopy [11,12]. Otherwise, the other active sites is proposed to be [Li^+O^-] centers which cannot be detected by Raman spectroscopy [12,13]. Figures 2(1)–(3) exhibit the Raman peaks of pure MgO (fresh) and 2%Li_2O/MgO (fresh and used) catalysts, respectively. In these figures, the Raman spectrum of Li_2O_2 is characterized at the wavenumber range of 794–860 cm^{-1} and broad band at about 259 cm^{-1} [12]. The band at 794–860 cm^{-1} is attributed to the internal O-O symmetric stretching mode of the peroxide species (O_2^{2-}) whilst that at 259 cm^{-1} is attributed to an external lattice vibration [12]. The slight Raman band at 1086 cm^{-1} and strong band at 761 cm^{-1} (Figure 2(3)) are attributed to Li_2CO_3 [12] possibly due to the adsorption of gaseous carbon dioxide on [Li^+O^-] centers to form [$Li^+CO_3^-$] during the reaction. The Raman band at 1086, 689 and 761 cm^{-1} are assigned to the symmetric stretching and antisymmetric bending modes of the carbonate ions, respectively indicating the presence of crystalline Li_2CO_3 on the catalyst surface after exposing the catalyst to the reactant gases (CH_4 and CO_2). The Raman spectra in the bands of 575 (Figure 2(2)), 500 and 426 cm^{-1} (Figure 2(3)) are ascribed to the presence of crystalline Li_2O species [12]. The disappearance of the peaks at about 259 and 826 cm^{-1} in Figure 2(3) indicate the decomposition of Li_2O_2 species, and consequently, the new sharp peak at 500 cm^{-1} and broad band at 426 cm^{-1} are attributed to the decomposition of Li_2O_2 to form Li_2O during the reaction.

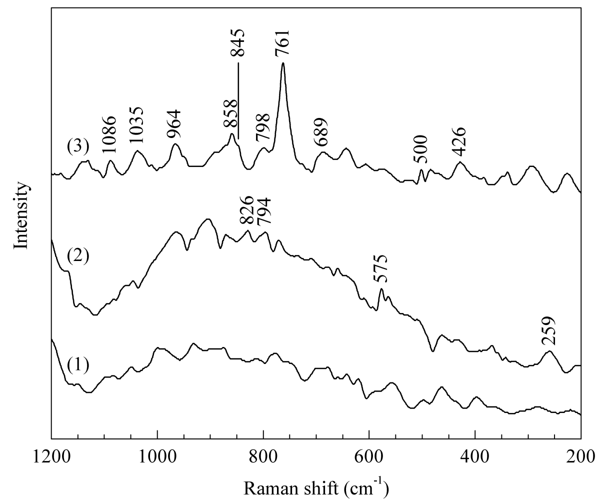

Figure 2. Raman spectra of MgO and Li_2O/MgO catalysts

(1) Pure MgO (fresh), (2) 2%Li_2O/MgO (fresh), (3) 2%Li_2O/MgO (used)

Figure 3 reveals the presence of active sites and metal oxides structures on 3%WO_3/1%Li_2O/MgO catalyst using Raman scattering. In this figure the fresh and used 3%WO_3/1%Li_2O/MgO catalyst are compared to both 1%Li_2O/MgO and pure MgO catalysts. The Raman spectrum of Li_2O_2 is characterized by the very slight peak at 798 cm^{-1} and the stronger peak at 816 cm^{-1} corresponding to the active species of O_2^{2-} on all the catalysts [12]. Next, the presence of crystalline Li_2O on the catalyst surface is detected at the Raman shifts of 422 (sharp), 510 and 520 cm^{-1} for ternary metal oxides as exhibited in Figures 3(3) and (4). Li_2CO_3 is detected to be present on the used catalyst (Figure 3(4)) at slight shift of about 751 cm^{-1} due to the interaction of Li_2O and gaseous CO_2 during the reaction. The strong Raman band at 918 cm^{-1} due to symmetric W-O stretching vibration [17] revealed the presence of [WO_4] tetrahedral species, while the slight band at about 279 cm^{-1} showed W-O-W deformation attributed to the crystalline WO_3. The Raman band at 553 cm^{-1} shows a W=O stretching vibration which is attributed to the [WO_6] octahedral unit [17]. The weak peak at 980 cm^{-1} is also attributed to W-O stretching vibration which may be assigned to the crystalline $MgWO_4$ [17]. The W-O bending vibration detected at 355 (Figure 3(3)) and 353 cm^{-1} (Figure 3(4)) are probably due to the distortion of the [WO_4] tetrahedral structure.

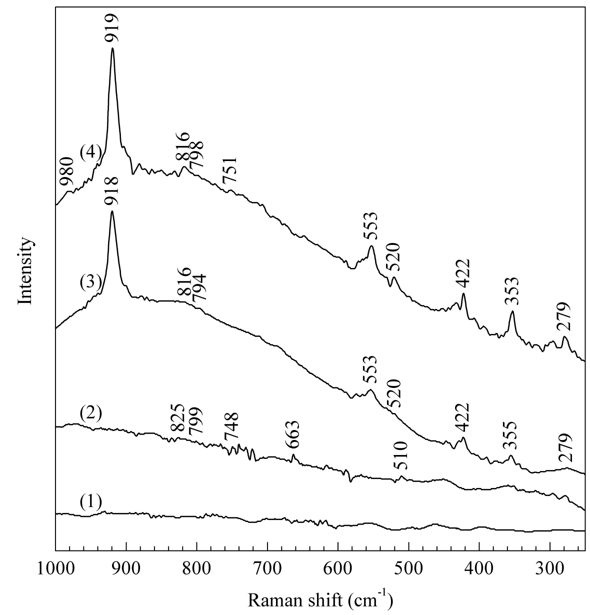

Figure 3. Raman spectra of MgO, Li_2O/MgO and WO_3/Li_2O/MgO catalysts

(1) Pure MgO (fresh), (2) 1%Li_2O/MgO (fresh), (3) 3%WO_3/1%Li_2O/MgO (fresh), (4) 3%WO_3/1%Li_2O/MgO (used)

In addition, FT-IR spectra of various weight percent of Li_2O-doped MgO catalysts are compared to pure MgO as depicted in Figure 4. The infra red band located at about 460–430 cm^{-1} is attributed to the antisymmetric stretching vibration of Li-O which is assigned to [LiO_4] tetrahedral [18,19]. From Figure 4, increasing the Li_2O content in the Li_2O/MgO catalysts gradually from 1% to 5% provides the different absorbances of infra red peaks in the range of 550–450 cm^{-1}. Initially, a strong and broad peak at 546 cm^{-1} was observed for 1%Li_2O/MgO catalyst, but the peak became weak and very broad and eventually shifted to a lower wavenumber of 507 cm^{-1} as observed in Figures 4(2)–(4).

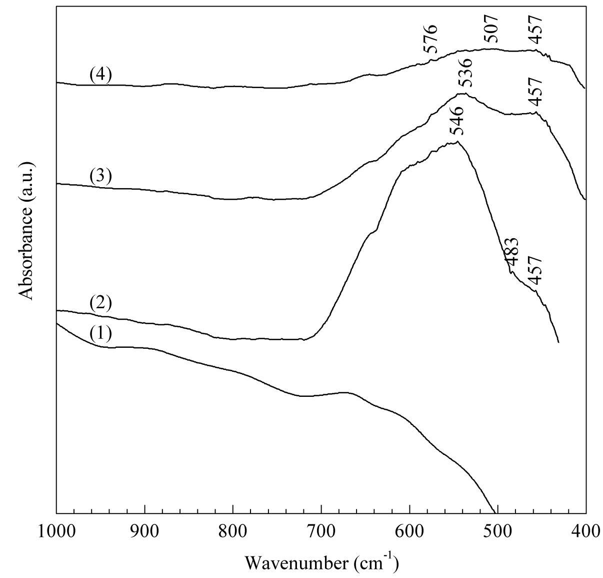

Figure 4. FT-IR spectra of MgO and Li_2O/MgO catalysts

(1) MgO, (2) 1%Li_2O/MgO, (3) 2%Li_2O/MgO, (4) 5%Li_2O/MgO

In Figure 5, the contrasting difference in the FT-IR spectroscopies of 1%Li_2O/MgO and 3%WO_3/1%Li_2O/MgO are obvious. The spectrum shows broad band at wavenumber range of 862–817 cm^{-1} which can be ascribed to W=O stretching vibration of octahedral [WO_6] [20], while the weak and sharp band at 688 cm^{-1} is ascribed to O-W-O stretching vibration [20]. The infra red spectra at 432 cm^{-1} (broad band) is ascribed to Li-O stretching vibration which is assigned to tetrahedral [LiO_4] [18,19]. The different peaks between Li_2O/MgO catalyst and WO_3-modified Li_2O/MgO catalyst are attributed to the dispersion of tungsten oxide-based crystalline phase in the Li_2O/MgO catalyst.

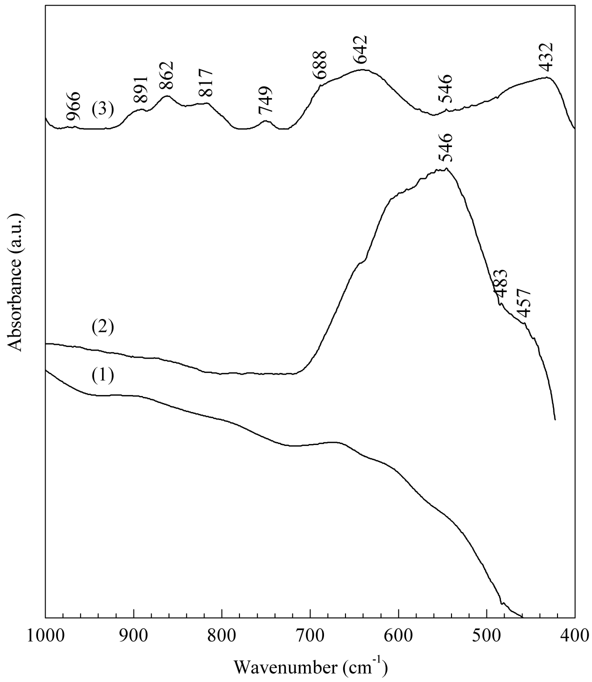

Figure 5. FT-IR spectra of MgO, Li_2O/MgO and WO_3/Li_2O/MgO catalysts

(1) MgO, (2) 1%Li_2O/MgO, (3) 3%WO_3/1%Li_2O/MgO

3.2. CeO_2-based catalysts screening suitable for CO_2-OCM

For CeO_2-based catalysts, the screening results of the various catalyst compositions with respect to C_{2+} hydrocarbons selectivity and yield as well as methane conversion are revealed in Table 4. Among the CeO_2-based catalysts, 5%MnO/15%CaO/CeO_2 gives the most promising results for CO_2-OCM. Over the catalyst, 5.3%, 3.3% and 62.2% of methane conversion, C_{2+} hydrocarbons yield and selectivity, respectively are achieved. The result is attributed to the presence of crystalline CaO on the CeO_2 catalyst as revealed by Raman spectroscopy, and is similar to the results reported previously [5–7]. The larger basicity of the base catalyst enhances carbon dioxide adsorption. The concentrations of oxygen vacancies increase with more CaO doped to the CeO_2-based catalysts. Thus, the oxygen ion conductivity increases strongly through the substitution where Ca^{2+}-ions (ionic radius 0.106 nm) are placed on the Ce^{4+}-sites (ionic radius 0.102 nm) under the formation of Ca''_{Ce}-ions, with charge compensation by oxygen vacancies [13].

Table 4. Catalysts performance results of CeO_2-based catalyst

Catalysts	CH_4 conversion (%)	CO selectivity (%)	C_{2+} hydrocarbons	
			Selectivity (%)	Yield (%)
CeO_2	13.0	87.8	19.4	2.4
15%CaO/CeO_2	2.7	25.0	75.0	2.0
5%MnO/CeO_2	8.8	96.9	3.1	0.3
5%MnO/15%CaO/CeO_2	5.3	37.8	62.2	3.3
3%WO_3/15%CaO/CeO_2	5.9	46.9	53.1	3.1

As presented in Table 4, pure CeO_2 catalyst exhibits decent methane conversion, but low C_{2+} hydrocarbons selectivity. Addition of CaO (alkaline earth) to the pure CeO_2 catalyst results in a significant increase in the C_{2+} hydrocarbon selectivity from 19.4% to 75%, but the methane conversion reduces significantly from 13% to 2.7% leading to a low C_{2+} hydrocarbons yield owing to a low methane conversion.

Doping 5% of MnO to the pure CeO_2 catalyst leads to methane conversion and C_{2+} hydrocarbons selectivity being reduced from 13% and 19.4% to 8.8% and 3.1%, respectively. The addition of 5%MnO species to the 15% CaO/CeO_2 catalyst increases C_{2+} hydrocarbons yield from 2.0% to 3.3% and methane conversion from 2.7% to 5.3%, respectively. However, the C_{2+} hydrocarbons selectivity reduces from 75.0% to 62.2%. The enhancement in the yield as a result of doping 5%MnO to 15%CaO/CeO_2 catalyst is possibly due to the synergistic effect of the transition metal (MnO) and rare-earth alkaline (CeO_2) by increasing their reducibilities which in turn enhance the oxygen vacancies formation. The doping of WO_3 to form a ternary metal oxide catalyst also contributes to a higher yield and selectivity compared to pure CeO_2 or bimetal oxide catalyst (Table 4). Indeed, the surface basicity of a catalyst contributes to a higher C_{2+} hydrocarbon selectivity due to the synergistic effect from the combination of CeO_2, alkaline earth (CaO) and transition metal (MnO or WO_3) [6,7,10] in which CaO has an important role. According to previous researchers, the CaO species is suggested to play an important role in CO_2 chemisorption on the catalyst surface [6], while the MnO species increases the reducibility of CeO_2 due to increasing oxygen mobility of CeO_2 catalyst which enhances its reducibility and produces more oxygen vacancies [7]. In general, MnO_x are compounds with a berthollide structure that contain labile lattice oxygen [21]. Their catalytic properties are attributed to the capacity for manganese to form oxides with variable oxidation states (MnO_2, Mn_2O_3, Mn_3O_4 or MnO) and to their oxygen storage capacity in the crystalline lattice. Due to its labile oxidation state, Mn is capable of playing the role of either a reducing agent or an oxidizing agent, acting in both cases as an active component of the redox system. Increase dispersion of the MnO_x on the support surface led to significant enhancement in the catalytic activity [21].

The Raman spectra of Mn-based catalysts namely pure CeO_2, 5%MnO/CeO_2 and 5%MnO/15%CaO/CeO_2 peaks are compared in Figure 6 and listed briefly in Table 5 including the corresponding vibration modes and structures. The Raman spectra of pure CeO_2 as well as CeO_2 as a support show the most intense band in the range of 400–500 cm^{-1} with the strongest and sharp band at 466 cm^{-1} which is assigned to the presence of a fluorite-type structure [12,17] and is a characteristic of crystalline CeO_2. From Figures 6(2) and 6(3), it is shown that Raman spectroscopy may not be powerful and suitable to detect the presence of metal oxides peaks when manganese oxide is doped on the catalysts although the laser powers were varied. The difficulties in detecting Mn-based peaks of the catalysts by Raman spectroscopy may be due to a relatively good dispersion of manganese oxide (MnO_x) on CeO_2 support causing an insensitive detection or, otherwise, due to the formation of amorphous manganese species. However, the presence and structure of manganese-doped ceria-based catalysts can also be revealed by FT-IR spectroscopy.

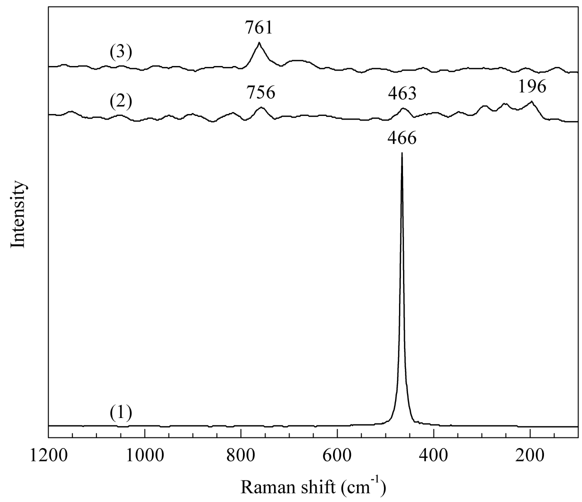

Figure 6. Raman spectra of the fresh CeO_2, MnO/CeO_2 and MnO/CaO/CeO_2 catalysts

(1) CeO_2 (fresh), (2) 5%MnO/CeO_2 (fresh),
(3) 5%MnO/15%CaO/CeO_2

Table 5. Resume of Raman and FT-IR spectra of various CeO_2-based catalysts

Materials	Band positions (cm^{-1})		Vibration modes	Structures	Ref.
	Raman	FT-IR			
Pure CeO_2	466	464, 535	—	crystalline CeO_2	[12,17]
CeO_2 as support	466	471	Ce-O vibration	crystalline CeO_2	[26]
	466	417, 418, 535	Ce-O vibration	crystalline CeO_2	[24]
15%CaO/CeO_2	732–726, 803	—	—	crystalline CaO	—
	—	875	O-Ca-O symmetric and Ca-O-Ca antisymmetric	crystalline CaO	[25]
	—	856	—	monodentate carbonate of Ca	[26]
3%WO_3/15%CaO/CeO_2	912	—	W-O symmetric stretching	[WO_4] tetrahedral	[17]
	804	—	W-O symmetric & W-O-W antisymmetric	[WO_6] octahedral	[17,18]
	—	805	W=O stretching	tungsten oxide-based	[22]
	—	712, 713	O-W-O stretching	tungsten oxide-based	[22]
	333	—	W-O bending	[WO_4] tetrahedral	[17]
	249	—	W-O-W deformation	crystalline WO_3	[17,20]
5%MnO/10%CaO/CeO_2	—	516	O-Mn-O antisymmetric	MnO_2 octahedral structure	[19,21,27]
	—	575	Mn-O-Mn stretching	MnO_2 octahedral structure	[19,21,27]
	—	465, 457	Mn-O-Mn deformation	MnO_2 octahedral structure	[27]

The Raman peaks of manganese oxides are very weak even for well-crystallized compounds of MnO_2, Mn_2O_3 and MnO, in which the Raman spectra of 756, 761 and 530 cm^{-1} are assigned to MnO_2, while the Raman peak of 196 $cm^{-1}$is attributed to MnO as revealed in Figures 6(2) and (3) [22]. The main contributions are attributed to the stretching mode of octahedral [MnO_6]. The Raman peaks at lower frequencies are attributed to the deformation modes of metal-oxygen chain of Mn-O-Mn in the octahedral structure of MnO_2 lattice. The weak and sharp infra red spectra at wavenumber of 516 and 575 cm^{-1}as revealed in Figures 7(2) and (3) are assigned to the antisymmetric stretching vibration modes of O-Mn-O and Mn-O vibration for MnO_2 octahedral structure, respectively [18,19,22,23]. The bulk phases of manganese oxide can also be identified physically by color. In fact, the black catalyst powder was identified to be the MnO_2 phase of fresh catalysts which changed to grey MnO and/or brown Mn_3O_4 during the CO_2-OCM reaction [23]. The physical identification of the manganese phases coincides with the results from FT-IR characterization in Figure 7. The lower wavenumber of

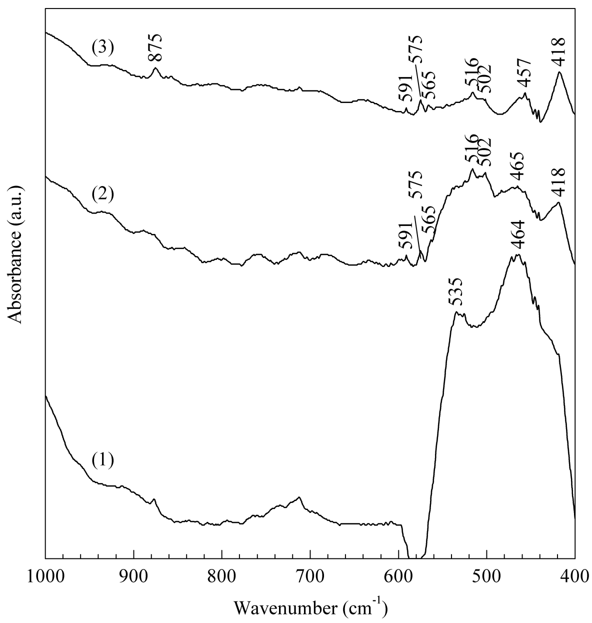

Figure 7. FT-IR spectra of CeO_2, MnO/CeO_2 and $MnO/CaO/CeO_2$ catalysts
(1) CeO_2, (2) 5%MnO/CeO_2, (3) 5%MnO/15%CaO/CeO_2

465 and 457 $cm^{-1}$are due to the deformation vibration mode of Mn-O-Mn which is assigned to the octahedral structure of MnO_2 lattice [22]. The calcium ions incorporation into the channels provide the lattice distortion and partial reduction of the manganese ions which results in a shifting of the vibrational mode frequencies from 465 to 457 cm^{-1} as depicted in Figures 7(2) and (3) [22]. The weak and sharp IR band at 875 cm^{-1} is assigned to the symmetric stretching vibration of O-Ca-O and antisymmetric stretching of Ca-O-Ca which is attributed to the presence of crystalline CaO [24].

The effect of adding tungsten oxide to 15%CaO/CeO_2 catalyst is also tested in the CO_2-OCM reaction as revealed in Table 4. The 3%WO_3 doping on the 15%CaO/CeO_2 catalyst decreases the C_{2+} hydrocarbons selectivity from 75.0% to 53.1%, while the yield is improved significantly due to a significant improvement in methane conversion from 2.7% to 5.9%. The results imply that tungsten may have a lower basicity than manganese species in which the catalyst basicity has an important role in C_{2+} hydrocarbons selectivity. Doping transition metals such as tungsten (0.065 nm) or manganese (0.091 nm) on CeO_2 (Ce^{4+} ionic radius of 0.102 nm) is suggested to cause a decrease in the crystal size of ceria thus, prevents sintering at high temperatures and at the same time increases the surface and bulk reducibility due to increasing oxygen mobility leading to a higher methane oxidation activity. However, the details of the interaction between ceria and tungsten/manganese species are not revealed in this study.

Figure 8 exhibits Raman spectra for CeO_2-based catalysts including their effect of tungsten doping. The Raman spectra for pure CeO_2 and CeO_2 as a support show the most intense band between 400–500 cm^{-1} with the strongest and sharp band at 466 cm^{-1} assigned to the presence of a fluorite type structure [12,17], and is a characteristic of crystalline CeO_2. Intensities of the Raman spectra for the crystalline Ca-based oxides are presented in the band range of 700–850 cm^{-1} (Figures 8(2) and (3)). The characteristic bands at 726, 732 and 803 cm^{-1} are ascribed to the crystalline CaO based on comparison between CaO/CeO_2 and pure CeO_2 catalysts. From Figure 8(3), the Raman bands at 912 and 333 cm^{-1} are due to W-O symmetric stretching and W-O bending vibrations modes, respectively [17], while the slight band at 249 cm^{-1} corresponds to W-O-W deformation vibration mode [25]. Consequently, the stretching band at 912 and 333 cm^{-1} are commonly used to characterize [WO_4] tetrahedral species, while the slight band at 249 cm^{-1} is ascribed to the crystalline WO_3 [17]. The W-O symmetric and W-O-W antisymmetric stretching are characterized at Raman band of 804 cm^{-1} which is ascribed to the

[WO_6] octahedral species [17,26]. However, this band may be overlapped with Raman peaks of crystalline CaO species. Monotungstate compounds made up of [WO_4] tetrahedral are indicated in the bands range of 910–1061 cm^{-1} (W-O symmetric stretching) and 300–400 cm^{-1} (antisymmetric stretching and bending modes). Isopolytungstate compounds, consisting of [WO_6] octahedral are posing bands in the range of 740–980 cm^{-1} (W-O symmetric and W-O-W antisymmetric stretching) [17,26].

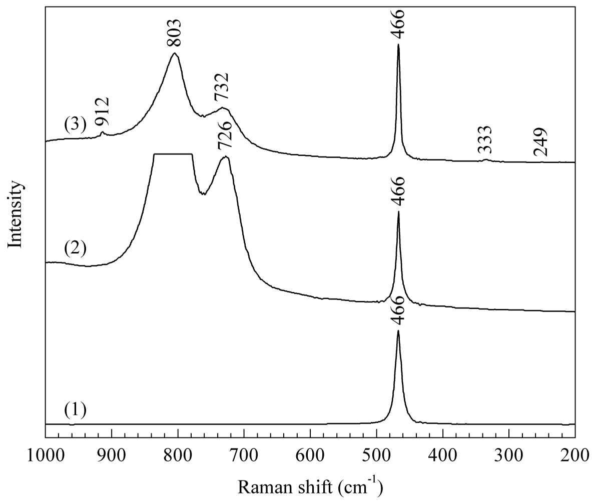

Figure 8. Raman spectra of the fresh CeO_2, CaO/CeO_2 and $WO_3/CaO/CeO_2$ catalysts

(1) CeO_2 (fresh), (2) 15%CaO/CeO_2 (fresh),
(3) 3%WO_3/15%CaO/CeO_2 (fresh)

Figure 9 shows the infra red spectra of pure CeO_2, binary metal oxide of 15%CaO/CeO_2 catalyst and ternary metal oxide of 3%WO_3/15%CaO/CeO_2 catalyst. The infra red spectra of pure CeO_2 is assigned to strong and broad bands at 535 and 464 cm^{-1} (Figure 9(1)) ascribed to Ce-O lattice vibration [24]. These peaks diminished when tungsten oxide and calcium oxide were doped. The infra red band at about 464 cm^{-1} for CeO_2 catalyst decreased its strength and shifted to higher wavenumber (471 cm^{-1}) after doping with CaO and WO_3. The weak band at 418 cm^{-1} and broad band at 535 cm^{-1} are assigned to fundamental Ce-O vibration [27]. Figure 9(2) depicts the FT-IR spectra recorded a strong and sharp peak at 875 cm^{-1} ascribed to CaO crystalline [28]. The weak absorption band at 856 cm^{-1} is assigned to the monodentate carbonate species of calcium [29]. Figure 9(3) shows the infra red characteristic of WO_3 doping influence to CaO/CeO_2 catalyst. The IR spectrum exhibits a strong and broad band at wavenumber of 805 cm^{-1} of W=O stretching vibration which can be assigned to the presence of tungsten oxide-based species [19]. The weak absorption band at 712 cm^{-1} is ascribed to O-W-O stretching vibration of tungsten oxide-based species [19].

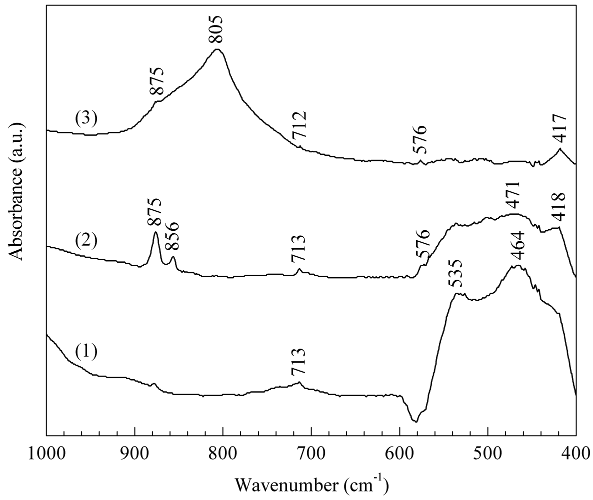

Figure 9. FT-IR spectra of CeO_2, CaO/CeO_2 and $WO_3/CaO/CeO_2$ catalysts

(1) CeO_2, (2) 15%CaO/CeO_2, (3) 3%WO_3/15%CaO/CeO_2

4. Conclusions

Binary metal oxide catalysts containing Li_2O and MgO are more suitable to catalyze the CO_2-OCM reaction due to several factors involving the catalyst basicity and ionic radius of the catalyst components. The addition of transition metals to the Li_2O/MgO catalyst did not improve the catalyst activity. One of the active sites of the Li_2O/MgO catalyst is proposed to be peroxide (O_2^{2-}) of Li_2O_2 and O^- of the [Li^+O^-] centers. Increasing the amount of Li_2O content doped into the MgO catalyst higher than 2% led to the formation of Li_2CO_3 or [$Li^+CO_3^-$] centers during the reaction. Hence, the [Li^+O^-] centers and Li_2O_2 formation are not enhanced as the carbonate centers cover the active sites of the catalyst and reduce its activity.

Increasing CaO doping to the CeO_2-based catalysts increases the concentration of oxygen vacancies and thus the oxygen ion conductivity through the substitution reaction where Ca^{2+}-ions are placed on Ce^{4+}-sites under the formation of Ca''_{Ce}-ions. The presence of crystalline CaO on the CeO_2-based catalyst has an important role in enhancing carbon dioxide adsorption by increasing the catalyst basicity. The high reducibility of the CeO_2 catalyst, an important factor in the CO_2-OCM catalyst activity, may be enhanced by the presence of manganese oxide species which increases oxygen mobility inside the catalyst and indeed produces more oxygen vacancies.

Basic metal oxides are suggested to be suitable catalysts for the selective oxidative coupling of methane to C_{2+} hydrocarbons using carbon dioxide as an oxidant. The performance of 5%MnO/15%CaO/CeO_2 catalyst is the most potential among the CeO_2-based catalysts, although lower than the 2%Li_2O/MgO catalyst. The 2%Li_2O/MgO catalyst showed the most promising C_{2+} hydrocarbons selectivity and yield at 98.0% and 5.7%, respectively. The presence of bulk crystalline phase and metal oxide structures as well as certain active sites on the MgO-based and the CeO_2-based catalysts are revealed by Raman and FT-IR spectroscopies. For the MgO-based catalyst, the peroxide (O_2^{2-}) of Li_2O_2 and O^- of the [Li^+O^-] centers are essential in increasing the catalyst activity, while for the CeO_2-based catalysts, the reducibility strength is important. From this study, it is apparent that the synergistic effects of various metals in a catalyst can help improve the CO_2-OCM catalytic process.

Acknowledgements

One of the authors (Istadi) would like to thank the Ministry of Science, Technology and Environment, Malaysia for the financial support received under the Project No 02-02-06-0016 EA099. We would also like to thank Dr. Agus Setyo Budi and Mr. Putut Marwoto of the Physics Department, Universiti Teknologi Malaysia for their help and discussion about Raman and FT-IR spectroscopies. The authors would also like to express their gratitudes to Assoc. Prof. Dr. Rosli Hussin for allowing the usage of Raman and FT-IR instruments in the Laboratorium of Material Analysis, Physics Dept., Universiti Teknologi Malaysia.

References

[1] Suhartanto T, York A P E, Hanif A *et al.* *Catal Lett*, 2001, **71**: 49
[2] Asami K, Fujita T, Kusakabe K *et al.* *Appl Catal A*, 1995, **126**: 245
[3] Asami K, Kusakabe K, Ashi N *et al.* *Appl Catal A*, 1997, **156**: 43
[4] Wang Y, Ohtsuka Y. *Appl Catal A*, 2001, **219**: 183
[5] Wang Y, Takahashi Y, Ohtsuka Y. *Appl Catal A*, 1998, **172**: L203
[6] Wang Y, Takahashi Y, Ohtsuka Y. *J Catal*, 1999, **186**: 160
[7] Wang Y, Ohtsuka Y. *J Catal*, 2000, **192**: 252
[8] Cai Y, Chou L, Li S *et al.* *Catal Lett*, 2003, **86**: 191
[9] Chen C L, Xu Y D, Lin G J *et al.* *Catal Lett*, 1996, **42**: 149
[10] Choudhary V R, Mulla S A R, Uphade B S. *Fuel*, 1999, **78**: 427
[11] Johnson M A, Stefanovich E V, Truong T N. *J Phys Chem B*, 1997, **101**: 3196
[12] Yang X. [PhD Dissertation], Texas: Texas A&M University, 1995
[13] Gellings P J, Bouwmeester H J M. *Catal Today*, 2000, **58**: 1
[14] Wach I E. *Catal Today*, 1996, **27**: 437
[15] Chen Y, Wach I E. *J Catal*, 2003, **217**: 468
[16] Mestl G. *J Mol Catal A*, 2000, **158**: 45
[17] Bigey C, Hilaire L, Maire G. *J Catal*, 2001, **198**: 208
[18] Julien C M, Massot M. *Mater Sci Eng B*, 2003, **100**: 69
[19] Julien C M, Massot M. *Mater Sci Eng B*, 2003, **97**: 217
[20] Gotić M, Ivanda M, Popović S *et al.* *Mater Sci Eng B*, 2000, **77**: 193
[21] Craciun R, Nentwick B, Hadjivanov K *et al.* *Appl Catal A*, 2003, **243**: 67
[22] Banov B, Momchilov A, Massot M *et al.* *Mater Sci Eng B*, 2003, **100**: 87
[23] Cadus L E, Ferretti O. *Appl Catal A*, 2002, **233**: 239
[24] Omran Z A, Mohamed M M. *Mater Chem Physics*, 2002, **77**: 704
[25] Valigi M, Gazzoli D, Pettiti I *et al.* *Appl Catal A*, 2002, **231**: 159
[26] Bothe-Almquist C L, Ettireddy R P, Bobst A *et al.* *J Catal*, 2000, **192**: 174
[27] Binet C, Daturi M, Lavalley J C. *Catal Today*, 1999, **50**: 207
[28] Maiti G C, Baerns M. *Appl Catal A*, 1995, **127**: 219
[29] Appel L G, Eon J G, Schmal M. *Catal Lett*, 1998, **56**: 199